Atomic force and scanning tunneling microscopy imaging of graphene nanosheets derived from graphite oxide

J.I. Paredes*, S. Villar-Rodil, P. Solís-Fernández, A. Martínez-Alonso, J.M.D. Tascón

Instituto Nacional del Carbón, CSIC, Apartado 73, 33080 Oviedo, Spain

* Corresponding author. Telephone number: (+34) 985 11 90 90. Fax number: (+34) 985 29 76 62. E-mail address: paredes@incar.csic.es

Abstract

Graphene nanosheets produced in the form of stable aqueous dispersions by chemical reduction of graphene oxide and deposited onto graphite substrates have been investigated by atomic force and scanning tunneling microscopy (AFM/STM). The chemically reduced graphene oxide nanosheets were hardly distinguishable from their unreduced counterparts in the topographic AFM images. However, they could be readily discriminated through phase imaging in the attractive regime of tapping mode AFM, probably due to differences in hydrophilicity arising from their distinct oxygen contents. The chemically reduced nanosheets displayed a smoothly undulated, globular morphology on the nanometer scale, with typical vertical variations in the subnanometer range and lateral feature sizes of ~5-10 nm. Such morphology was attributed to be the result of significant structural disorder in the carbon skeleton, which originates during the strong oxidation that leads to graphene oxide and remains after chemical reduction. Direct evidence of structural disorder was provided by atomic-scale STM imaging, which revealed an absence of long-range periodicity in the graphene nanosheets. Only structured domains a few nanometers large were observed instead. Likewise, the nanosheet edges appeared atomically rough and ill-defined, though smooth on the nanometer scale. The unreduced graphene oxide nanosheets could only be imaged by STM at very low tunneling currents (~1 pA), being visualized in some cases with inverted contrast relative to the graphite substrate, a result that was attributed to their extremely low conductivity. Complementary characterization of the unreduced and chemically reduced nanosheets was carried out by thermogravimetric analysis as well as UV-vis absorption, X-ray photoelectron and Raman spectroscopies. In particular, the somewhat puzzling Raman results were interpreted to be the result of an amorphous character of the graphene oxide material.

1. Introduction

Interest in graphene in the fields of condensed matter physics and materials science has been rapidly growing over the last few years as a result of its first successful isolation[1,2] and the subsequent discovery of new and unusual fundamental physical properties, which mainly originate from its two-dimensional nature.[3-8] In parallel with these developments from the basic science perspective, many applications have been proposed and are currently being explored for graphene and some of its chemically modified forms (most notably, those derived from graphite oxide), including their use in nanoelectronic devices,[1,9-12] electrically conductive and mechanically reinforced composite materials,[13,14] gas sensors,[15,16] supercapacitors,[17] Li-ion batteries,[18] or drug delivery.[19]

Chemically modified graphene derived from graphite oxide is particularly attractive for materials science applications, as it can be conveniently processed in liquid phase in bulk quantities, thus facilitating the preparation of, e.g., ultrathin films,[11,12,16,20] paper-like materials[21-23] or composites.[13,14,24] More specifically, due to the hydrophilicity and ionizability of many of its oxygen-containing functional groups, graphite oxide can be readily exfoliated in water to yield stable dispersions of single-layer sheets (graphene oxide sheets).[13,25,26] These dispersions constitute a strategic starting point for the large-scale production of graphene, which is typically achieved by chemical or thermal reduction.[9,11-13,16,18,20,23,25-30] For instance, it has very recently been reported that aqueous dispersions of electrically conductive graphene nanosheets exhibiting long-term stability can be prepared via chemical reduction of the non-conductive graphene oxide dispersions without the aid of surfactants or any other stabilizers.[26] However, it has also been recognized that such chemically derived graphene differs significantly from its pristine, defect-free counterpart, which is usually produced by micromechanical

cleavage of bulk graphite.[1-3] In particular, chemically reduced graphene oxide is thought to contain, apart from residual oxygen functionalities, a significant amount of structural disorder inherited from the oxidative transformation of graphite to graphite oxide,[11,25,27,28] even though direct microscopic information in this respect has so far not been documented. Thus, for the further advancement of materials based on this chemically modified form of graphene, an in-depth knowledge of its local nanometer- and atomic-scale structure would be highly desirable.

Here, we report the use of atomic force and scanning tunneling microscopies (AFM/STM) to probe the local characteristics (nanometer-scale morphology and atomic-scale structure) of graphene nanosheets produced as stable aqueous dispersions by chemical reduction of the corresponding graphene oxide dispersions. To date, AFM has been employed for the most part to examine only general features (i.e., sheet thickness and lateral dimensions) of pristine or chemically modified graphene sheets,[2,10,11,13,25,29] and much less frequently to image its detailed nanoscale morphology,[31,32] which has not been undertaken for the specific case of chemically reduced graphene oxide. Detailed AFM images of the so-called functionalized graphene sheets (FGSs) have been previously reported,[31] but these constitute a different type of chemically modified graphene to that documented here. FGSs are prepared through rapid thermal expansion at 1050 ºC of graphite oxide, whereas the graphene nanosheets studied here are produced by chemical reaction with a reducing agent (hydrazine) at low temperature. Therefore, structural and chemical differences could be expected between both types of graphene. Likewise, atomic-scale STM studies of graphene are rather scarce and, again, these concern only pristine samples prepared by micromechanical cleavage,[32-34] epitaxial growth[35,36] or STM lithography,[37] but not samples prepared by chemical reduction of graphene oxide. This is, to the best of our knowledge, the first

report that provides direct structural information down to the atomic scale for such type of graphene.

2. Experimental

The graphene nanosheets investigated in this work were produced in the form of stable dispersions in water following the procedure recently reported by Li *et al*,[26] which consists of three steps: 1) synthesis of graphite oxide from pristine graphite powder, 2) exfoliation and dispersion in water of the graphite oxide product as single-layer sheets (graphene oxide sheets), and 3) conversion of the graphene oxide sheets back to graphene by controlled chemical reduction. Graphite oxide was prepared from natural graphite powder (Fluka 50870) via the Hummers method using $NaNO_3$, H_2SO_4 and $KMnO_4$.[38,39] The oxidized material was purified by washing with 10% HCl solution, repeatedly rinsing with copious amounts of Milli-Q water and filtering through standard filter paper with a Büchner funnel, after which a thick graphite oxide slurry was obtained. To make dispersions in water, either the graphite oxide slurry was directly used or, alternatively, a dried graphite oxide powder was employed. The latter was prepared by drying the slurry under vacuum (80 ºC, 3 h), peeling the resulting ~0.5 mm thick film off the filter paper and gently grinding it with a mortar and pestle. In a typical exfoliation process, a small amount of the graphite oxide slurry or dried powder was added to a given volume of water and sonicated in an ultrasound bath cleaner (JP Selecta Ultrasons system, 40 kHz) for 1 h. Then, the sonicated dispersion was centrifuged (Eppendorf 5424 microcentrifuge) at 20238 *g* for 20 min to remove unexfoliated graphite oxide particles, and the supernatant, which was the final graphene oxide dispersion, was collected. Subsequent characterization of the dispersions by different techniques did not yield significant differences between those derived from the

slurry and from the dried powder. Chemical reduction of the dispersed graphene oxide sheets was carried out by reaction with hydrazine monohydrate after adjusting the pH of the dispersion to ~10 with ammonia to promote the colloidal stability of the sheets through electrostatic repulsion. As such stability also critically depends on the amount of reducing agent employed in relation to the mass of graphene oxide present in the dispersion,[26] it was necessary to work with graphene oxide dispersions of known concentration, for which UV-vis absorption spectroscopy was employed. A calibration curve relating absorbance at 231 nm (see below for the choice of such wavelength) and graphene oxide concentration was obtained by measuring the absorbance for different dispersions of known concentration (prepared by sonication of the dried powder). Reduction was typically accomplished for graphene oxide dispersions with a concentration of 0.1 mg ml^{-1}, using 2 μL of 25% ammonia solution and 0.1 μL of hydrazine monohydrate for each mL of graphene oxide dispersion, which has been reported as the optimal ratio for reduction.[26] The reaction was carried out in a water bath at 95 ºC for 1 h.

A general characterization of the graphene oxide material before and after chemical reduction, in dispersed state or processed into solid films (depending on the technique used), was performed by UV-vis absorption spectroscopy, thermogravimetric analysis (TGA), X-ray photoelectron spectroscopy (XPS) and Raman spectroscopy. The films were prepared either in the form of substrate-supported ultrathin coatings or as free-standing paper-like materials. In the former case, the dispersion was cast dropwise onto a pre-heated (~60-70 ºC) flat metallic disk until a uniform dark film covering the whole substrate was visible to the naked eye. Unreduced and chemically reduced graphene oxide paper was produced, as reported elsewhere,[21,22] by filtering the corresponding aqueous dispersion through an Anodisc membrane filter 47 mm in diameter and 0.2 μm

of pore size (Whatman). UV-vis absorption spectra of the dispersions were recorded with a double-beam Heλios α spectrophotometer, from Thermo Spectronic. TGA of the free-standing paper was accomplished by means of an SDT Q600 thermobalance (TA Instruments) under Ar gas flow (100 mL min^{-1}) at a heating rate of 10 ºC min^{-1}, using Pt crucibles. For XPS measurement of the paper samples, a SPECS system working under 10^{-7} Pa with a monochromatic Al Kα X-ray source (100 W) was employed. The surface charging effect observed for the non-conductive, unreduced graphene oxide sample was corrected by the use of an electron flood gun operating at 0.4 eV and 0.10 mA.[39] Surface composition (atomic %) of the samples was determined from the survey spectra by considering the integrated intensities of the main XPS peaks of the elements that were found. Raman measurements were made with a Horiba Jobin-Yvon LabRam instrument at a laser excitation wavelength of 532 nm.

For the AFM and STM investigations, the unreduced and chemically reduced graphene oxide aqueous dispersions were drop-cast onto freshly cleaved, atomically flat highly oriented pyrolytic graphite (HOPG) substrates (ZYH grade, from Advanced Ceramics Corporation) and then allowed to dry in air at room temperature. The dispersions were also deposited onto freshly cleaved mica (grade V-1, Electron Microscopy Sciences) and the nanosheets displayed by AFM a similar appearance to that of the sheets deposited onto HOPG. However, as mica is electrically non-conductive, it cannot be employed for STM studies. For this reason, in the present work HOPG was the substrate of choice and all the presented results were obtained on this material. AFM and STM were carried out under ambient conditions (relative humidity ~40%, temperature ~22-24 ºC) with a Nanoscope IIIa Multimode apparatus (Veeco Instruments). AFM was performed in the tapping mode of operation using rectangular silicon cantilevers with spring constant of ~40 N m^{-1} and typical resonance frequencies

between 250 and 300 kHz. Imaging was accomplished in the attractive regime of tip-sample interaction,[40,41] recording height (topography) and phase images simultaneously. STM measurements were performed in the constant current mode (variable height) with mechanically prepared Pt/Ir (80/20) tips. To allow operation with tunneling currents down to the pA regime, a low-current converter was coupled to the Nanoscope IIIa system. Unless otherwise stated, the STM images presented here are height images.

3. Results and discussion

3.1. Global characterization of graphene dispersions and thin films

Fig. 1 (inset) shows a digital picture of 0.1 mg mL^{-1} graphene oxide dispersion in water (left), together with its chemically reduced counterpart (right). The yellow-brown color characteristic of the unreduced dispersion changes to black following reduction, suggesting that deoxygenation of the graphene nanosheets has effectively come about.[13,26] The picture was taken 5 months after preparation of both dispersions, and none of them shows any visible sign of precipitation, which indicates that both the unreduced and reduced dispersions possess long-term stability. Additional evidence for reduction is presented in the UV-vis spectra of Fig. 1. In agreement with previous reports,[26,39] the spectrum obtained for the unreduced graphene oxide dispersion (red plot) exhibits a maximum at 231 nm (attributed to $\pi \rightarrow \pi^*$ transitions of aromatic C-C bonds) and a shoulder at ~300 nm (ascribed to $n \rightarrow \pi^*$ transitions of C=O bonds). After reduction (black plot), the maximum redshifts to about 270 nm and a significant increase in absorbance is noticed for the whole range of wavelengths larger than 231 nm. Both effects are indication that electronic conjugation has been restored, at least to some extent, within the carbon framework of the graphene nanosheets.[26,42]

Further proof of the chemical transformations induced by reduction was obtained by TGA and XPS measurements. Fig. 2 shows the thermogravimetric (TG) and differential thermogravimetric (DTG) plots for the unreduced graphene oxide material (full and dotted orange curves, respectively) and the reduced material (full and dotted black curves, respectively). For the unreduced material, the main mass loss (~30%) occurs around 200 ºC, and is attributed to the decomposition of labile oxygen functional groups.[25,39] The mass loss at temperatures below 100 ºC (~15%) can be ascribed to the removal of adsorbed water, whereas the steady loss observed for temperatures above 300 ºC and up to 1000 ºC, which amounts to ~20%, is assigned to the release of more stable oxygen functionalities.[39] Following reduction, the sharp mass loss around 200 ºC is no longer observed, suggesting that the labile oxygen functional groups in graphene oxide are largely removed by reaction with hydrazine. On the other hand, a slow, steady mass loss (~20%) over the whole temperature range above 100 ºC is retained after reduction, which implies that the more stable oxygen functionalities are not eliminated from graphene by the chemical reduction. The reduced material also displays a significant mass loss (~10%) below 100 ºC due to water desorption. The presence of oxygen on both samples was directly evidenced by XPS. Fig. 3 presents high resolution core-level C 1s spectra for the unreduced graphene oxide material (a) and its reduced counterpart (b). For the unreduced material, a complex band showing two maxima ~2 eV apart can be noticed. This band was fitted to three components, located at 284.6 (graphitic C=C species), 286.6 (C-O species) and 287.9 eV (C=O species), as reported previously.[39] It has been suggested that defect (sp^3) C-C species give rise to a component very close to 286.6 eV,[43,44] so in the present case it is very likely that the 286.6 eV component also bears a contribution from these species. After reduction, the relative contribution of the components associated to oxygenated and sp^3 carbon species

was seen to decrease very significantly (Fig. 3b, see also Table 1), which agrees with previous reports from the literature.[11,25,26,30,31] In this case, the C 1s band was fitted to 6 components, located at 284.6 (graphitic C=C species), 285.5 (localised alternant hydrocarbon),[43] 286.3 (C-O, C-N[45] and sp^3 carbon species), 287.4 (C=O and $\pi \rightarrow \pi^*$ shake up peak of band centred at 285.5 eV), 288.8 (COOH), and 290.0 eV ($\pi \rightarrow \pi^*$ shake up peak of band centred at 284.6 eV). Deoxygenation of the graphene nanosheets by the chemical reduction process was also evidenced from the O/C atomic ratios derived from the XPS survey spectra (not shown), which yielded values of 0.43 for the unreduced graphene oxide material and 0.16 for the reduced material. The residual oxygen functionalities retained following reduction would still render the nanosheets somewhat hydrophilic, imparting them with colloidal stability in water,[26] and also explaining the significant amount of water that this material is able to adsorb (see TG results, Fig. 2).

Raman spectroscopy was employed to obtain global structural information, as opposed to the local structural information that will be provided by atomic-scale STM, for the unreduced and chemically reduced samples. The results of the Raman measurements are presented in Fig. 4, which shows first- and second-order spectra. For comparison purposes, the spectrum of the pristine graphite powder used to prepare the chemically modified graphenes is included in Fig. 4a. The first-order spectrum of this pristine graphite is characterized by a strong band at ~1580 cm^{-1} (G band) and a very weak band at ~1340 cm^{-1} (D band). The latter is induced by structural disorder, in such a way that the integrated intensity ratio of the D and G bands (I_D/I_G) increases with the amount of disorder for graphitic materials, vanishing for completely defect-free graphite.[46] The second-order (two-photon) spectrum of the starting graphite sample is dominated by a strong band at ~2690 cm^{-1} (2D band) and a weak band at ~3240 cm^{-1}. The 2D band is the overtone (second harmonic) of the D band, whereas the band at

~3240 cm^{-1} corresponds to the overtone of a band located at ~1620 cm^{-1} (D´ band) in the first-order spectrum,[47] which in the present case is seen as a weak shoulder on the high wavenumber side of the G band in Fig. 4a. Similar to the case of the D band, the D´ band is not present in defect-free graphite and its relative intensity increases with graphitic disorder. Raman spectra of the chemically modified graphenes [Fig. 4 b (unreduced material) and c (reduced material)] were recorded for the thin solid film samples (both substrate-supported coating and free-standing paper; see Experimental section) as well as for the liquid samples (aqueous dispersions), without significant differences being detected between the spectra for the different preparations of the same material. As noticed from the spectrum of the unreduced graphene oxide material in Fig. 4b, the I_D/I_G ratio increases dramatically in comparison with that of the starting graphite material (from 0.13 to 1.46), implying that the oxidation process has introduced a considerable amount of structural disorder in the graphene lattice. The same conclusion can be drawn when the second-order spectrum is inspected. First, the 2D band is seen to broaden and decrease in relative intensity compared to the G band, an effect that has been related to the presence of defects in graphitic materials.[47] Second, a band appears at ~2920 cm^{-1}, partly obscuring the 2D band. This new band results from the combination of the two modes that give rise to the first-order D and G bands, and is caused by lattice disorder.[47] When the Raman spectrum of the chemically reduced material (Fig, 4c) is compared with that of the unreduced sample (Fig. 4b), subtle, rather than drastic, changes are observed. Even though the I_D/I_G ratio remains essentially constant (1.43 vs. 1.46 before reduction), the shape of the first-order spectrum has been altered to some extent. The G band of the chemically reduced material is somewhat asymmetric, displaying an intense shoulder on its high wavenumber side, which is not evident on the G band of the unreduced material. This shoulder could in principle

correspond to the D´ band located at ~1620 cm^{-1} previously discussed. Regarding the second-order spectrum, the 2D band appears more intense and defined in relation to the band at ~2920 cm^{-1} after chemical reduction (compare Fig. 4 c with b). Similar changes upon chemical reduction of graphene oxide have been recently documented by other groups,[23,25,27,30] even with an increased I_D/I_G ratio following reduction reported in one case.[25] This result is quite unexpected and apparently contradicts the idea that, after chemical reduction and subsequent restoration of the aromaticity on the graphene lattice, a significantly reduced D band might be anticipated. Stankovich *et al* interpret such result by assuming that reduction increases the number of aromatic domains of smaller overall size in graphene, which would lead to an enhancement of the I_D/I_G ratio.[25] However, if this interpretation was correct, a decrease in the 2D band relative to the band at ~2920 cm^{-1} should be likely expected after reduction,[47] which was not observed either in the present work (Fig. 4) or in previous ones.[30] We believe that the apparent contradiction can be solved by assuming that the carbon lattice in graphene oxide has developed some degree of amorphous character due to the oxidation process itself. Previous work with disordered and amorphous carbon materials has shown that, rather than increasing, the I_D/I_G ratio decreases upon amorphization of highly defected, but essentially graphitic, carbons, the effect being attributed to a large distortion of the 6-fold aromatic rings.[46] In such a case, the I_D/I_G ratio cannot be used as a measure of structural disorder and, accordingly, comparisons between materials of amorphous and graphitic character are no longer valid. Taking into account that the basal plane in graphene oxide is heavily decorated with oxygen functionalities such as epoxides and hydroxyls,[13,25,48] a significant distortion of the aromatic rings, and consequently a certain amorphous character, should be expected for this unreduced material. On the other hand, when the graphene oxide sheet is deoxygenated by the chemical reduction

process, the distortion of the 6-fold rings is removed and the carbon lattice returns to an essentially graphitic, but highly defected, state. Thus, an increase in the I_D/I_G ratio upon chemical reduction would even be possible.[25] We note that a similar amorphization phenomenon has been recently invoked to interpret Raman spectroscopy and atomic-scale STM results of plasma-oxidized graphite.[49]

3.2. Local characterization of individual graphene nanosheets

Fig. 5 shows general height (a,c) and phase (b,d) tapping mode AFM images of unreduced (a,b) and chemically reduced (c,d) graphene oxide nanosheets deposited onto HOPG, as obtained in the attractive regime of tip-sample interaction. Typical line profiles taken along the marked red lines are also presented superimposed onto each image. Tapping mode AFM imaging was performed in the attractive regime with a two-fold purpose: first, to avoid any disturbance to the nanosheets by the AFM tip, as this regime has been proved to be extremely gentle in comparison not only with contact mode AFM but also with the repulsive regime of tapping mode;[41,50] second, to probe chemical differences between the unreduced and the reduced graphene oxide nanosheets. It has been previously shown that phase imaging in the attractive regime of tapping mode is able to locally detect the presence of hydrophilic, oxygen groups on carbon surfaces,[51-53] so a discrimination between the unreduced and reduced nanosheets based on phase images would in principle be possible. As the height images and corresponding line profiles show, there are no noticeable morphological differences between the unreduced (Fig. 5a) and chemically reduced (Fig. 5c) nanosheets at this magnification. In both cases, sheets of uniform height relative to the HOPG substrate (~1.0-1.2 nm) and lateral dimensions ranging from a few hundred nm to about 1 μm are observed. In accordance with previous reports,[13,25,26] these objects are interpreted to be

single-layer sheets. By contrast, significant differences between both samples were observed in the phase images. Since both the unreduced and reduced nanosheets were deposited onto freshly cleaved HOPG, this substrate served as a common reference against which the phase values of the sheets could be compared.[53] For the unreduced sheets (Fig. 5b), the measured phase was clearly different (~2-3º higher; see line profile) to that of the unoxidized, pristine HOPG surface, whereas the phase of the chemically reduced sheets was essentially the same as that of the substrate (Fig. 5d). For carbon surfaces, a phase shift upward of this magnitude relative to the pristine HOPG substrate can be interpreted as a signature of the presence of hydrophilic oxygen functionalities,[51-53] so its observation on the unreduced graphene oxide material constitutes local evidence of the strong oxidation of the sheets. Detailed inspection of the phase image in Fig. 5b reveals that while all the sheets display a generally increased phase relative to that of the HOPG background, there exist some local variations in the actual phase values from sheet to sheet or even within an individual sheet. This can be seen, for instance, when comparing the two sheets identified by black and white arrows in Fig. 5a and b. The sheet denoted by the black arrow exhibits a higher phase than that of the sheet marked by the white arrow. Such observations suggest that different graphene oxide sheets could be oxidized to somewhat different extents and that single sheets may exhibit areas with different levels of oxidation on the nanometer scale. On the other hand, the fact that the chemically reduced graphene oxide sheets present very similar phase values to that of the HOPG substrate (Fig. 5d) suggests that reduction has decreased the hydrophilicity of the sheets to a level closer (although most probably not identical) to that of the HOPG surface. This result could be certainly expected, as it has been shown that a dried dispersion of chemically reduced graphene oxide cannot be redispersed in

water (i.e., it is hydrophobic), whereas redispersion is possible for the dried, unreduced graphene oxide material.[21,26]

Fig. 6 shows tapping mode AFM images of individual sheets in more detail (a,b) and of the nanometer-scale morphology of the sheets at high magnification (c,d), together with typical line profiles (e,f) for the unreduced (a,c,e) and chemically reduced (b,d,f) graphene oxide nanosheets. The line profile in Fig. 6e (f) was taken along the white line marked in Fig. 6c (d). In general terms, the unreduced sheets as well as their chemically reduced counterparts display a rather smooth appearance (Fig. 6a and b), both in terms of z-scale roughness (see below) and sheet perimeter. In particular, we note that no significant spikes or crevices are observed along the sheet perimeter. On the nanometer scale, the sheets display a uniform globular or bumpy morphology with feature sizes ranging typically between 5 and 10 nm (Fig. 6c and d). Although such morphology is common to the unreduced and chemically reduced graphene oxide sheets, subtle differences between both samples regarding z-scale roughness become evident when their respective images, line profiles and RMS values are compared, the roughness being slightly larger for the unreduced sheets (RMS values of 0.108 nm vs. 0.095 nm for the unreduced and reduced nanosheets, respectively). In any case, even for the relatively rough unreduced graphene oxide sheets, the measured height variations are always in the subnanometer range (see Fig. 6e and f), indicating that the sheets are essentially flat objects. We tentatively interpret the slightly rough morphology of the sheets as a consequence of the structural disorder induced by oxidation (see Raman spectroscopy results) and maybe also of the presence of the oxygen functionalities themselves, which are probably not evenly distributed across the graphene surface.[27] As the amount of oxygen functional groups on the graphene surface is considerably diminished following chemical reduction (see XPS data), the possible roughness

induced by such groups should be accordingly smaller in the chemically reduced sheets, which would explain the reported differences between the unreduced and the reduced samples in Fig. 6c and d. We note that the sheets investigated here were deposited onto atomically flat surfaces (mainly HOPG, but also mica), so a contribution of the substrates to the observed topography of the sheets can be ruled out. This is different to many AFM studies of graphene, which use the technologically relevant (but atomically rough) SiO_2/Si substrate. In such case, even pristine, defect-free graphene exhibits some degree of roughness, and this has been attributed to the fact that the graphene sheet partially conforms to the corrugation of the underlying substrate.[32,33] We also note that the chemically reduced graphene oxide nanosheets appear to be structurally different to the functionalized graphene sheets (FGSs) reported elsewhere, which were also deposited onto atomically flat HOPG and studied by AFM.[31] The latter type of graphene was seen to display a significant number of wrinkles, attributed to line defects in the carbon lattice. As such type of feature was never observed in our chemically reduced nanosheets, we interpret that the wrinkles are the result of structural modifications during the high temperature (1050 ºC) treatment that the FGSs are subjected to.

Next, we discuss the results of the STM measurements. As could be anticipated due to their electrically non-conductive nature, it was not possible to image the unreduced graphene oxide nanosheets under tunneling conditions typically employed to study graphitic surfaces, i.e. using tunneling currents in the nA and sub-nA regime and bias voltages from a few tens to several hundreds of mV. Most probably, tunneling currents of such magnitude cannot flow through the unreduced nanosheets, with the consequence that they are swept away by the STM tip and only the conductive HOPG substrate is visualized, as it was indeed the case. An alternative explanation could be that the large number of functional groups on the graphene oxide sheets does not allow the latter to

come close enough to the HOPG substrate, so as to induce a significant Van der Waals interaction between nanosheet and substrate. Thus, if such interaction is too weak, the anisotropic electric field of the STM tip could sweep away the nanosheet. Indeed, this effect reportedly made the observation of functionalized carbon nanotubes very difficult.[54] In any case, the sheets became visible when the STM was operated under very low tunneling currents (~1 pA or below) and large bias voltages (~2000 mV). This is exemplified in Fig. 7a, which shows features (sheets) whose lateral dimensions are consistent with those observed in the AFM images of the same sample (Fig. 5a). It should also be noted that in some cases, depending on the tip used, the unreduced nanosheets were visualized with inverted contrast relative to the HOPG substrate. Fig. 7b shows an example of this type of image, which is characterized by the presence of a considerable number of dark features. Taking into account that the density, size and shape of such features is coincident with those of the graphene oxide nanosheets seen by AFM (Fig. 5a) and that the features were not observed on pristine HOPG onto which no dispersion was deposited, we conclude that they correspond to the nanosheets, which are imaged with inverted contrast relative to the HOPG substrate. As illustrated in the line profile of Fig. 7c, which was taken along the white line marked in Fig. 7b, the sheets are visualized with an apparent depth of ~0.5-1.0 nm below the HOPG surface. It is well known that both topography and electronic structure contribute to the image contrast in STM, which is due to the fact that the measured tunneling current over a given surface depends not only on the tip-sample separation but also on the local density of electronic states near the Fermi level of the sample surface.[55] Thus, for a very poorly conductive area of the surface (the graphene oxide sheets in the present case), the density of electronic states near the Fermi level is much smaller than that for a highly conductive region (the HOPG substrate), giving rise to lower tunneling currents over the

former. Alternatively, a lower tunneling current over the graphene oxide nanosheets could arise from a larger separation (and thus a lower tunneling probability) between the nanosheet and the HOPG substrate owing to the presence of a very large number of oxygen functionalities on the former. If one or both effects are large enough, as it appears to be here in some cases, they can completely counterbalance the topographical contribution to the tunneling current, resulting in the sheets being imaged with inverted contrast. However, these appear to be necessary but not sufficient conditions for the emergence of inverted contrast, as the latter is only observed with some specific tips. Thus, the characteristics of the STM tips also play a key role in the appearance of inverted contrast. Inverted contrast arising from electronic effects has been well documented in the STM literature of substrate-supported molecules and particles.[56-58] In this respect, we note that a similar effect to that observed here (contrast reversal depending on the tip used) has been reported for the STM imaging of purple membranes on HOPG and attributed to differences in the local geometry of the STM tips.[59]

Following chemical reduction, STM images of the nanosheets could be routinely achieved even at relatively high tunnelling currents (up to several nA) and low bias voltages (down to several mV) without inverted contrast, implying that the reduced nanosheets have become electrically conductive, as expected. Fig. 8a shows a general STM image that spans several nanosheets, their size and shape being consistent with those observed in the AFM images of the same sample (Fig. 5c). As measured by STM and exemplified in the averaged multiple profile of Fig. 8b, virtually all the nanosheets were ~0.6-0.8 nm high (relative to the HOPG substrate), while the overlapping areas of two or more nanosheets or the folded regions of a single sheet exhibited heights that were integer multiples of this value. Such value is noticeably smaller than that obtained by AFM for the same sample (1.0-1.2 nm). In the case of AFM, it has been speculated

that several factors, rather than just the actual sheet thickness, have an influence on the measured height of graphene or chemically modified graphene over a given substrate, in particular the different interaction of the AFM tip with the graphene sheet and with the substrate.[1,31,60,61] Regarding STM, it is also very likely that the tip interacts differently with the defective, chemically modified graphene nanosheets and with the pristine HOPG surface as a result of differences in their electronic structure. Indeed, a dramatic example in this respect was the inverted contrast observed for the unreduced graphene oxide nanosheets (Fig. 7a). Although these nanosheets become electrically conductive after chemical reduction, their conductivity has been shown to lag significantly behind that of pristine, defect-free graphene,[27] implying a somewhat different electronic structure to that of the latter. Furthermore, the tunneling geometry is more complex over the nanosheet than it is over the bare HOPG substrate.[62,63] All these effects could contribute to the apparent height (relative to the supporting substrate) measured by STM for the chemically reduced nanosheets. Likewise, taking into account that the nature of the tip-sample interaction used for imaging is very different in AFM and STM, it is not surprising that the two techniques lead to different values of sheet height relative to the HOPG substrate as a result of the mentioned contributions to the measured height. The main question raised in connection with these observations is that of the accurate measurement of the actual nanosheet thickness. Since in principle this cannot be done by measuring the nanosheet height relative to the supporting substrate because of the potential spurious contributions discussed above, it should be made by measuring the nanosheet height relative to another nanosheet (e.g., using two overlapping sheets), so that the possible influence of the tip interacting with objects of different nature is removed. With tapping mode AFM, this measurement should be ideally carried out in the attractive regime, rather than in the repulsive one, as only the former is minimally

invasive.[41] In the repulsive regime, sample deformation, which could affect the measured heights, cannot be ruled out, and the deformation could be different for the overlapping and non-overlapping areas of two nanosheets. When we measure (in the attractive regime) the height of the overlapping area between two sheets relative to the non-overlapping area, we obtain a value of ~1.0 nm for the unreduced graphene oxide nanosheets and ~0.6 nm for their chemically reduced counterparts. These values should in principle correspond to the actual thickness of the sheets, and are reasonable in that the reduced sheets turn out to be thinner than the unreduced ones, as expected due to the removal of a large majority of the oxygen functional groups. In line with the reasoning made in the case of AFM, the actual thickness of chemically reduced nanosheets should also be determined with STM by measuring the height of an overlapping area or folded region relative to the non-overlapping area or non-folded region of a nanosheet. Such height turned out to be ~0.7 nm, which is very close to that obtained independently by AFM (~0.6 nm), thus reinforcing the idea that 0.6-0.7 nm is the actual thickness of the chemically reduced graphene oxide nanosheets.

Fig. 8c shows the detailed nanometer-scale morphology of the chemically reduced graphene oxide nanosheets as imaged by STM. A line profile displaying the typical height variations across the nanosheets is also presented (Fig. 8d). In comparing this and other STM images of similar magnification with their AFM counterparts (e.g., Fig. 8c vs. 6d), we see that there is a good agreement between the general morphology visualized by the two techniques (both unveil the same type of globular/bumpy feature), although finer structural detail is provided by STM (for instance, concerning the shape of the bumps). This higher resolving power on the nanoscale is probably due to the fact that the tips used for STM are somewhat sharper than those used for AFM. In any case, the strong similarity between the STM and AFM results suggests that the contrast

observed in the nanometer scale images by STM (Fig. 8c) is mainly of topographic origin. Thus, although local variations of electronic structure are also present to some extent within the nanosheet, they probably play only a secondary role in the features observed at such magnification. Thus, we can safely conclude that chemically reduced graphene oxide nanosheets display a smoothly undulated morphology even on an atomically flat substrate such as HOPG, probably as a result of the distortions induced on the carbon lattice by residual functional groups and structural defects.

Direct evidence for the presence of structural disorder in the chemically reduced nanosheets was obtained by atomic-scale STM imaging. Some representative results are shown in Fig. 9. In general terms, these images are characterized by a complete lack of long-range atomic-scale order. Rather, atomic-sized spots arranged into different local domains are the dominant feature. At most, such domains constitute clearly ordered patterns a few nm large, whereas in other cases the local order of the atomic-sized spots is less evident or even absent. An example of a relatively large ordered domain can be seen in the bottom right part of Fig. 9a, along with smaller domains in the same image. A line profile taken from the large domain (white line) is presented in Fig. 9b. From this profile, a peak-to-peak distance between spots of ~0.22-0.24 nm was measured, which is very close to the ~0.25 nm periodicity observed in the triangular pattern that is typically obtained in the atomic-scale STM images of pristine, defect-free HOPG (Fig. 9c). We note that not every area of the nanosheets investigated on the atomic scale displayed clearly ordered domains such as those seen in Fig. 9a. In many cases, as mentioned before, the atomic-sized spots were not arranged into any recognizable domain (e.g., bottom part of Fig. 9d) or were arranged into domains without evident periodicity (Fig. 9e). Obviously, this is an indication that structural disorder in the chemically reduced nanosheets is not spatially uniform. On the contrary, local areas

exhibiting a high degree of structural imperfection (Fig. 9d and e) coexist with relatively ordered regions (Fig. 9a). The structural disorder unveiled by STM on the reduced nanosheets (and also by Raman spectroscopy; Fig. 4c) can in principle be attributed to the presence of oxygen functionalities covalently attached to the basal plane of the graphene sheet, which remain in significant quantities after chemical reduction (see XPS data), as well as to large numbers of atomic-scale defects within the carbon lattice itself, which were presumably created during the oxidation and/or reduction processes. At present, the exact nature of such defects in the graphene nanosheets is not known. One possibility is that they correspond to atomic vacancies, which would have originated via abstraction of carbon atoms by oxygen in the oxidation or reduction step, giving rise to volatile CO or CO_2. Isolated atomic vacancies on an otherwise defect-free graphitic surface are visualized by STM as defined protrusions between one and a few nm large,[51,64] but the STM signature of a very large concentration of vacancies, which would probably be the case here, has not been clearly established. Nevertheless, atomic-scale STM images reported for HOPG surfaces aggressively modified by microwave oxygen plasma treatment (which is known to proceed via atomic vacancy creation) revealed extremely disordered structures not very different to those obtained here for the chemically reduced nanosheets.[49] An alternative scenario to explain the presence of structural defects in the reduced graphene nanosheets would be a strong distortion (corrugation) of the carbon lattice as a result of the preparation of graphite oxide. Szabó *et al* have recently proposed a structural model for graphite oxide in which the carbon skeleton of the graphene layers becomes highly corrugated and deformed due to the grafting of large amounts of oxygen functional groups.[48] Corrugation of (unreduced) graphene oxide was evident in the AFM images obtained here (Fig. 6c). It is plausible that such corrugation/deformation of the graphene

lattice persists to a certain degree after removal of most of the oxygen by chemical reduction, as overcoming an energy barrier (and, therefore, some thermal annealing) would probably be required to resume a perfectly flat, pristine graphene structure from the corrugated one. In the present work, corrugation of the chemically reduced graphene oxide nanosheets was evident from the AFM images (Fig. 6d) as well as from both the nanometer- and atomic-scale STM images (Fig. 8c and 9). Corrugation/deformation of the carbon lattice would probably give rise to a distortion of the atomic-scale features seen in the STM images (Fig. 9). From the previous discussion, it is reasonable to conclude that both atomic vacancies and corrugation of the carbon skeleton are possibly present in the chemically reduced graphene oxide nanosheets. We also note that an in-depth understanding of the atomic-scale features reported in Fig. 9 would most probably require the assistance of some theoretical modeling. However, in the present case this could be a difficult task. Theoretical modeling of the STM images can be reasonably carried out for isolated, individual atomic-scale defects,[65] so that simulated STM images of potential defect structures can be compared with the experimental ones. However, the investigated graphene nanosheets presumably contain several different types of unknown defects, which are present in unknown (but very high) densities and with unknown spatial distributions. As defect type, density and spatial distribution are all known to affect the atomic-scale STM images of graphitic surfaces,[66] the modeling task could become exceedingly arduous.

Finally, the detailed structure of the edges of the chemically reduced nanosheets was also investigated by STM. For pristine graphene, especially in the form of nanoribbons, the edge structure has been shown to play an important role in its electronic properties.[37] In the present case of graphene nanosheets prepared as stable aqueous dispersions, the sheet edges are thought to be randomly decorated with carboxyl groups that favor the

stability of the colloidal dispersion via electrostatic repulsion.[13,26] Furthermore, taking into account that (1) the basal surface of the graphene nanosheets was highly disordered on the atomic scale (Fig. 9) and (2) the cutting of the nanosheets during sonication is a rather uncontrolled process, we expect the nanosheet edges to be atomically rough and ill-defined. This is confirmed by the images of Fig. 10. Fig. 10a shows a nanometer-scale STM image of a nanosheet edge. As discussed previously in connection with the AFM images, the edges appear smooth and straight at this relatively low magnification. However, as illustrated in Fig. 10b (graphene nanosheet: left; HOPG substrate: right), the edge profile is rather rough on the atomic scale, indicating that even the straight sections of the sheet edge (Fig. 10a) do not possess a well defined crystallographic orientation. Fig. 10c presents an atomic-scale image of a nanosheet corner, exhibiting a very disordered, ill-defined structure that contrasts with the crystallinity of the HOPG substrate surrounding it. This is further highlighted in the line profile of Fig. 10d, which was taken along the white line in Fig. 10c: the periodicity observed over the HOPG substrate (left part of the profile) is completely lost when moving onto the nanosheet (right part). It will be interesting to see how these structures evolve and graphitic order is restored when the nanosheets are subjected to heat treatment, which will be the subject of future studies.

4. Conclusions

Atomic force and scanning tunneling microscopies (AFM/STM) have afforded a direct visualization of the nanometer-scale morphology and atomic-scale structure of graphene nanosheets produced by chemical reduction of graphene oxide dispersions. In general terms, we can conclude that the structure of these chemically derived nanosheets is significantly different to that of pristine graphene prepared by

micromechanical cleavage of bulk graphite. Even when deposited on an atomically flat substrate such as graphite, the former display an undulated, globular morphology that can be attributed to distortions of the carbon skeleton induced by the strong oxidation employed to produce such type of graphene. Atomic-scale STM imaging provided direct evidence of the lattice distortion in these graphene nanosheets, as long-range periodicity was never seen. Only ordered domains a few nanometers large could be identified. Such observation was consistent with the results obtained by Raman spectroscopy, which also indicated the presence of considerable structural disorder. Atomically rough and ill-defined nanosheet edges were also visualized by STM. Although they possess an extremely low electrical conductivity, the unreduced graphene oxide nanosheets could be imaged by STM, but only working with tunneling currents in the pA regime. In this case, the sheets appeared sometimes with inverted contrast in the images. Finally, phase imaging in the attractive regime of tapping mode AFM could be employed to discriminate between the unreduced and chemically reduced graphene oxide nanosheets. Significant differences in hydrophilicity between the two samples that result from distinct oxygen levels probably allow such discrimination to be made.

Acknowledgements

Partial funding of this work by MEC (project CTQ2005-09105-C04-02) and CSIC (I3 project 200680I198) is gratefully acknowledged. P.S.-F. also acknowledges receipt of an I3P pre-doctoral contract from CSIC.

References

(1) Novoselov, K. S.; Geim, A. K.; Morozov, S. V.; Jiang, D.; Zhang, Y.; Dubonos, S. V.; Grigorieva, I. V.; Firsov, A. A. *Science* **2004**, *306*, 666-669.

(2) Novoselov, K. S.; Jiang, D.; Schedin, F.; Booth, T. J.; Khotkevich, V. V.; Morozov, S. V.; Geim, A. K. *Proc. Natl. Acad. Sci. USA* **2005**, *102*, 10451-10453.

(3) Geim, A. K.; Novoselov, K. S. *Nature Mater.* **2007**, *6*, 183-191.

(4) Fasolino, A.; Los, J.H.; Katsnelson, M. I. *Nature Mater.* **2007**, *6*, 858-861.

(5) Miao, F.; Wijeratne, S.; Zhang, Y.; Coskun, U. C.; Bao, W.; Lau, C. N. *Science* **2008**, *317*, 1530-1533.

(6) Chen, J.-H.; Jang, C.; Adam, S.; Fuhrer, M. S.; Williams, E. D.; Ishigami, M. *Nature Phys.* **2008**, *4*, 377-381.

(7) Li, Z. Q.; Henriksen, E.A.; Jiang, Z.; Hao, Z.; Martin, M. C.; Kim, P.; Stormer, H. L.; Basov, D. N. *Nature Phys.* **2008**, *4*, 532-535.

(8) Martin, J.; Akerman, N.; Ulbricht, G.; Lohmann, T.; Smet, J. H.; von Klitzing, K.; Yacoby, A. *Nature Phys.* **2008**, *4*, 144-148.

(9) Gilje, S.; Han, S.; Wang, M.; Wang, K. L.; Kaner, R.B. *Nano Lett.* **2007**, *7*, 3394-3398.

(10) Li, X.; Wang, X.; Zhang, L.; Lee, S.; Dai, H. *Science* **2008**, *319*, 1229-1232.

(11) Eda, G.; Fanchini, G.; Chhowalla, M. *Nature Nanotech.* **2008**, *3*, 270-274.

(12) Wang, X.; Zhi, L.; Müllen, K. *Nano Lett.* **2008**, *8*, 323-327.

(13) Stankovich, S.; Dikin, D.A.; Dommett, G. H. B.; Kohlhaas, K. M.; Zimney, E. J.; Stach, E. A.; Piner, R. D.; Nguyen, S. T.; Ruoff, R. S. *Nature* **2006**, *442*, 282-286.

(14) Ramanathan, T.; Abdala, A. A.; Stankovich, S.; Dikin, D. A.; Herrera-Alonso, M.; Piner, R. D.; Adamson, D. H.; Schniepp, H. C.; Chen, X.; Ruoff, R.S.; Nguyen, S. T.; Aksay, I. A.; Prud´homme, R. K.; Brinson, L. C. *Nature Nanotech.* **2008**, *3*, 327-331.

(15) Schedin, F.; Geim, A. K.; Morozov, S. V.; Hill, E. W.; Blake, P.; Katsnelson, M. I.; Novoselov, K. S. *Nature Mater.* **2007**, *6*, 652-655.

(16) Robinson, J. T.; Perkins, F. K.; Snow, E. S.; Wei, Z.; Sheehan, P. E. *Nano Lett.* **2008**, *8*, 3137-3140.

(17) Stoller, M. D.; Park, S.; Zhu, Y.; An, J.; Ruoff, R. S. *Nano Lett.* **2008**, *8*, 3498-3502.

(18) Yoo, E. J.; Kim, J.; Hosono, E.; Zhou, H.; Kudo, T.; Honma, I. *Nano Lett.* **2008**, *8*, 2277-2282.

(19) Liu, Z.; Robinson, J. T.; Sun, X.; Dai, H. *J. Am. Chem. Soc.* **2008**, *130*, 10876-10877.

(20) Becerril, H.A.; Mao, J.; Liu, Z.; Stoltenberg, R. M.; Bao, Z.; Chen, Y. *ACS Nano* **2008**, *2*, 463-470.

(21) Dikin, D. A.; Stankovich, S.; Zimney, E. J.; Piner, R. D.; Dommett, G. H. B.; Evmenenko, G.; Nguyen, S. T.; Ruoff, R. S. *Nature* **2007**, *448*, 457-460.

(22) Chen, H.; Müller, M. B.; Gilmore, K. J.; Wallace, G. G.; Li, D. *Adv. Mater.* **2008**, *20*, 3557-3561.

(23) Xu, Y.; Bai, H.; Lu, G.; Li, C.; Shi, G. *J. Am. Chem. Soc.* **2008**, *130*, 5856-5857.

(24) Verdejo, R.; Barroso-Bujans, F.; Rodriguez-Perez, M. A.; de Saja, J. A.; Lopez-Manchado, M. A. *J. Mater. Chem.* **2008**, *18*, 2221-2226.

(25) Stankovich, S.; Dikin, D. A.; Piner, R. D.; Colas, K. A.; Kleinhammes, A.; Jia, Y.; Wu, Y.; Nguyen, S. T.; Ruoff, R. S. *Carbon* **2007**, *45*, 1558-1565.

(26) Li, D.; Müller, M. B.; Gilje, S.; Kaner, R. B.; Wallace, G. G. *Nature Nanotech.* **2008**, *3*, 101-105.

(27) Gómez-Navarro, C.; Weitz, R. T.; Bittner, A. M.; Scolari, M.; Mews, A.; Burghard, M.; Kern, K. *Nano Lett.* **2007**, *7*, 3499-3503.

(28) Wang, G.; Yang, J.; Park, J.; Gou, X.; Wang, B.; Liu, H.; Yao, J. *J. Phys. Chem. C* **2008**, *112*, 8192-8195.

(29) Si, Y. ; Samulski, E.T. *Nano Lett.* **2008**, *8*, 1679-1682.

(30) Park, S.; An, J.; Piner, R. D.; Jung, I.; Yang, D.; Velamakanni, A.; Nguyen, S. T.; Ruoff, R. S. *Chem. Mater.* **2008**, *20*, 6592-6594.

(31) Schniepp, H. C.; Li, J.-L.; McAllister, M. J.; Sai, H.; Herrera-Alonso, M.; Adamson, D. H.; Prud´homme, R. K.; Car, R.; Saville, D.A.; Aksay, I. A. *J. Phys. Chem. B* **2006**, *110*, 8535-8539.

(32) Ishigami, M.; Chen, J. H.; Cullen, W.G.; Fuhrer, M. S.; Williams, E. D. *Nano Lett.* **2007**, *7*, 1643-1648.

(33) Stolyarova, E.; Rim, K.T.; Ryu, S.; Maultzsch, J.; Kim, P.; Brus, L. E.; Heinz, T. F.; Hybertsen, M. S.; Flynn, G. W. *Proc. Natl. Acad. Sci. USA* **2007**, *104*, 9209-9212.

(34) Stolyarova, E.; Stolyarov, D.; Liu, L.; Rim, K. T.; Zhang, Y.; Han, M.; Hybersten, M.; Kim, P.; Flynn, G. *J. Phys. Chem. C* **2008**, *112*, 6681-6688.

(35) Rutter, G. M.; Crain, J. N. ; Guisinger, N. P.; Li, T.; First, P. N.; Stroscio, J. A. *Science* **2007**, *317*, 219-222.

(36) Mallet, P.; Varchon, F.; Naud, C.; Magaud, L.; Berger, C.; Veuillen, J.-Y. *Phys. Rev. B* **2007**, *76*, 041403.

(37) Tapasztó, L.; Dobrik, G.; Lambin, P.; Biró, L. P. *Nature Nanotech.* **2008**, *3*, 397-401.

(38) Hummers, W.; Offeman, R. *J. Am. Chem. Soc.* **1958**, *80*, 1339.

(39) Paredes, J. I.; Villar-Rodil, S.; Martínez-Alonso, A.; Tascón, J. M. D. *Langmuir* **2008**, *24*, 10560-10564.

(40) James, P. J.; Antognozzi, M. ; Tamayo, J.; McMaster, T. J.; Newton, J. M.; Miles, M. J. *Langmuir* **2001**, *17*, 349-360.

(41) Paredes, J. I.; Villar-Rodil, S.; Tamargo-Martínez, K.; Martínez-Alonso, A.; Tascón, J. M. D. *Langmuir* **2006**, *22*, 4728-4733.

(42) Skoog, D. A.; Holler, F. J.; Nieman. T. A. *Principles of Instrumental Analysis*; Hartcourt Brace & Company: Philadelphia, 1998; Chapter 13.

(43) Yang, D.-Q.; Rochette, J.-F.; Sacher, E. *Langmuir* **2005**, *21*, 8539-8545.

(44) Yang, D.-Q.; Sacher, E. *Langmuir* **2006**, *22*, 860-862.

(45) Wang, Q.; Kaliaguine, S.; Ait-Kadi, A. *J. Appl. Polym. Sci.* **1993**, *48*, 121-148.

(46) Ferrari, A. C.; Robertson, J. *Phys. Rev. B* **2000**, *61*, 14095-14107.

(47) Chieu, T. C. ; Dresselhaus, M. S.; Endo, M. *Phys. Rev. B* **1982**, *26*, 5867-5877.

(48) Szabo, T.; Berkesi, O.; Forgo, P.; Josepovits, K.; Sanakis, Y.; Petridis, D.; Dekany, I. *Chem. Mater.* **2006**, *18*, 2740-2749.

(49) Paredes, J. I.; Martínez-Alonso, A.; Tascón, J. M. D. *Langmuir* **2007**, *23*, 8932-8943.

(50) San Paulo, A.; García, R. *Biophys. J.* **2000**, *78*, 1599-1605.

(51) Paredes, J. I.; Martínez-Alonso, A.; Tascón, J. M. D. *Langmuir* **2002**, *18*, 4314-4323.

(52) Paredes, J. I.; Martínez-Alonso, A.; Tascón, J. M. D. *Chem. Commun.* **2002**, 1790-1791.

(53) Paredes, J. I.; Martínez-Alonso, A.; Tascón, J. M. D. *Langmuir* **2003**, *19*, 7665-7668.

(54) Kónya, Z.; Vesselenyi, I.; Niesz, K.; Kukovecz, A.; Demortier, A.; Fonseca, A.; Delhalle, J.; Mekhalif, Z.; Nagy, J.B.; Koós, A.A.; Osváth, Z.; Kocsonya, A.; Biró, L.P.; Kiricsi, I. *Chem. Phys. Lett.* **2002**, *360*, 429-435.

(55) Magonov, S. N.; Whangbo, M.-H. *Surface Analysis with STM and AFM*; VCH, Weinheim: Germany, 1996.

(56) Guo, Q.; Yin, J.; Palmer, R. E.; Bampos, N.; Sanders, J. K. M. *Chem. Phys. Lett.* **2005**, *402*, 121-125.

(57) MacLeod, J. M.; Miwa, R. H.; Srivastava, G. P.; Malean, A. B. *Surf. Sci.* **2005**, *576*, 116-122.

(58) Kim, D. H.; Shapir, E.; Jeong, H.; Porath, D.; Yi, J. *Phys. Rev. B* **2006**, 73, 235416.

(59) García, R.; Tamayo, J. *Langmuir* **1995**, 11, 2109-2114.

(60) Gupta, A.; Chen, G.; Joshi, P.; Tadigadapa, S.; Eklund, P. C. *Nano Lett.* **2006**, *6*, 2667-2673.

(61) Nemes-Incze, P.; Osváth, Z.; Kamarás, K.; Biró, L.P. *Carbon* **2008**, *46*, 1435-1442.

(62) Biró, L.P.; Gyulai, J.; Lambin, Ph.; Nagy, J.B.; Lazarescu, S.; Mark, G.I.; Fonseca, A.; Surján, P.R.; Szekeres, Zs.; Thiry, P.A.; Lucas, A.A. *Carbon* **1998**, *36*, 689-696.

(63) Mark, G.I.; Biró, L.P.; Gyulai, J.; Thiry, P.A.; Lucas, A.A.; Lambin, P. *Phys. Rev. B* **2000**, *62*, 2797-2805.

(64) Hahn, J. R.; Kang, H. *Phys. Rev. B* **1999**, *60*, 6007-6017.

(65) Amara, H.; Latil, S.; Meunier, V.; Lambin, Ph.; Charlier, J.-C. *Phys. Rev. B* **2007**, *76*, 115423.

(66) Ruffieux, P.; Melle-Franco, M.; Gröning, O.; Bielmann, M.; Zerbetto, F.; Gröning, P. *Phys. Rev. B* **2005**, *71*, 153403.

Table 1. Assignment of carbon species and their relative weight for unreduced and chemically reduced graphene oxide as obtained by fitting high resolution core-level C1s X-ray photoelectron spectra

Unreduced graphene oxide						
Binding energy (eV)	284.6		286.6	287.9		
Assignment	C=C		C-O sp^3 C-C	C=O		
% area	41.25		47.49	11.26		
Reduced graphene oxide						
Binding energy (eV)	284.6	285.5	286.3	287.4	288.8	290.0
Assignment	C=C	localised hydrocarb.	C-O C-N sp^3 C-C	C=O $\pi \rightarrow \pi^*$	COOH	$\pi \rightarrow \pi^*$
% area	66.48	9.51	9.18	6.72	2.53	5.58

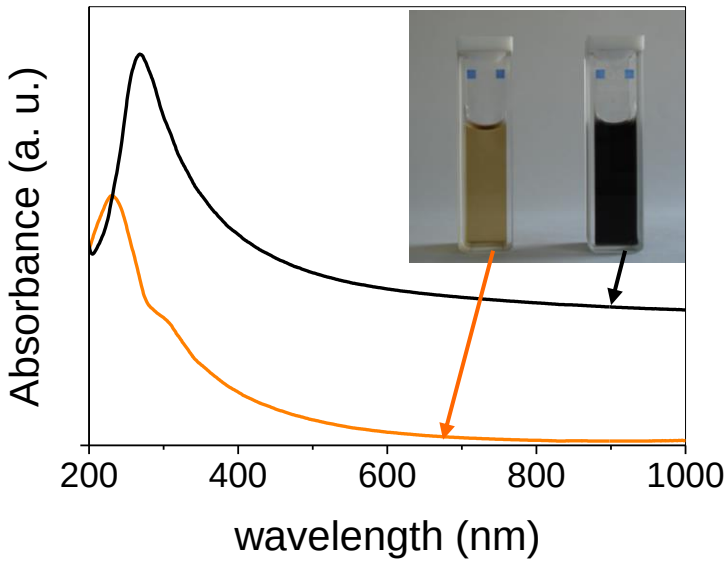

Fig. 1 UV-vis spectra for unreduced (orange) and chemically reduced (black) graphene oxide dispersions in water. Inset: digital picture of the unreduced (left) and reduced (right) aqueous dispersions.

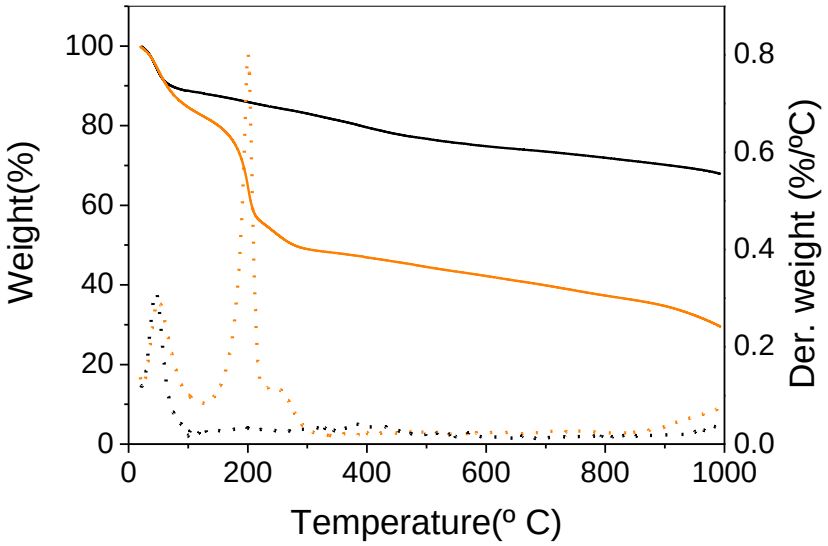

Fig. 2 TG (full curves) and DTG (dotted curves) plots for unreduced (orange) and chemically reduced (black) graphene oxide material.

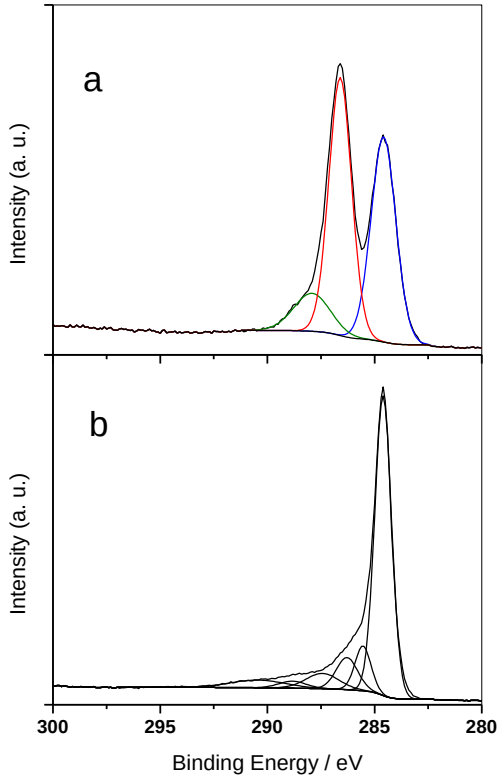

Fig. 3 High resolution C 1s X-ray photoelectron spectra for unreduced (a) and chemically reduced (b) graphene oxide material.

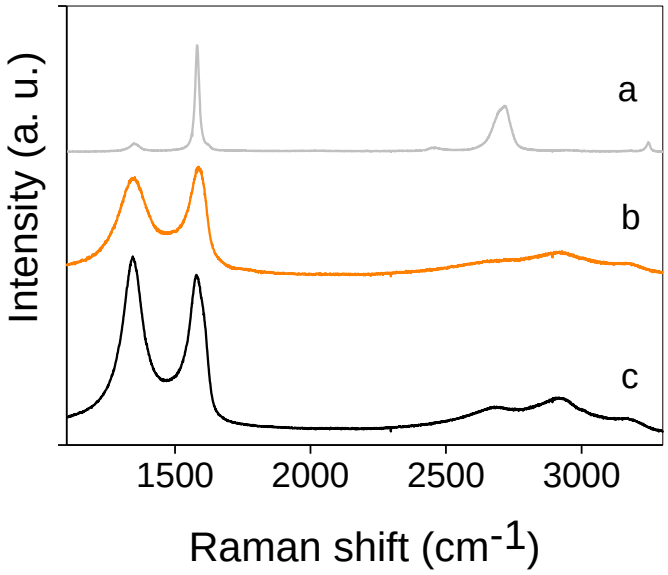

Fig. 4 Raman spectra for pristine natural graphite powder (a), unreduced graphene oxide film (b) and chemically reduced graphene oxide film (c).

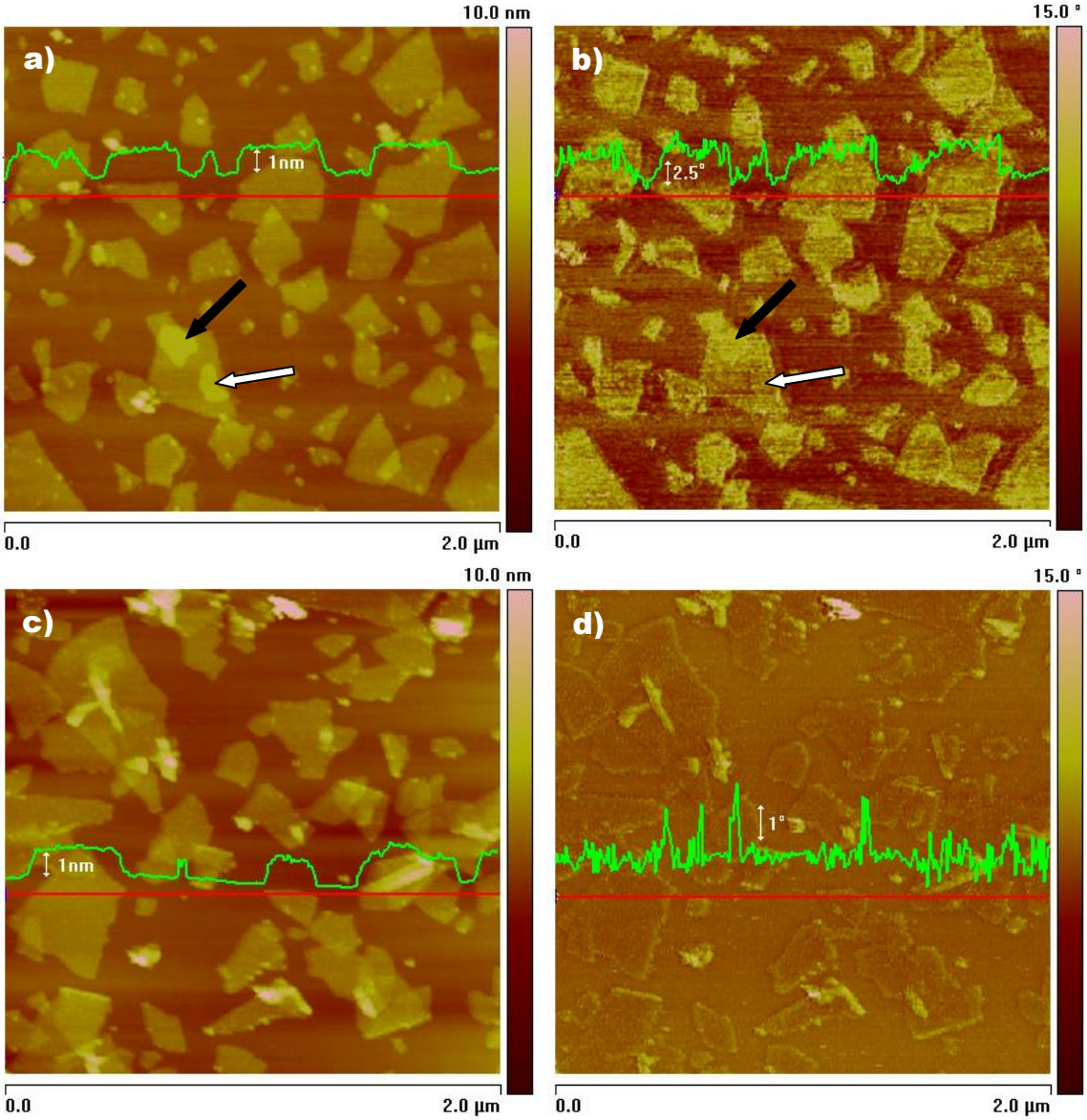

Fig. 5 Height (a,c) and corresponding phase (b,d) tapping mode AFM images of unreduced (a,b) and chemically reduced (c,d) graphene oxide nanosheets deposited from aqueous dispersions onto freshly cleaved HOPG. The images were recorded in the attractive regime of tip-sample interaction. Superimposed onto each image is a line profile taken along the marked red line.

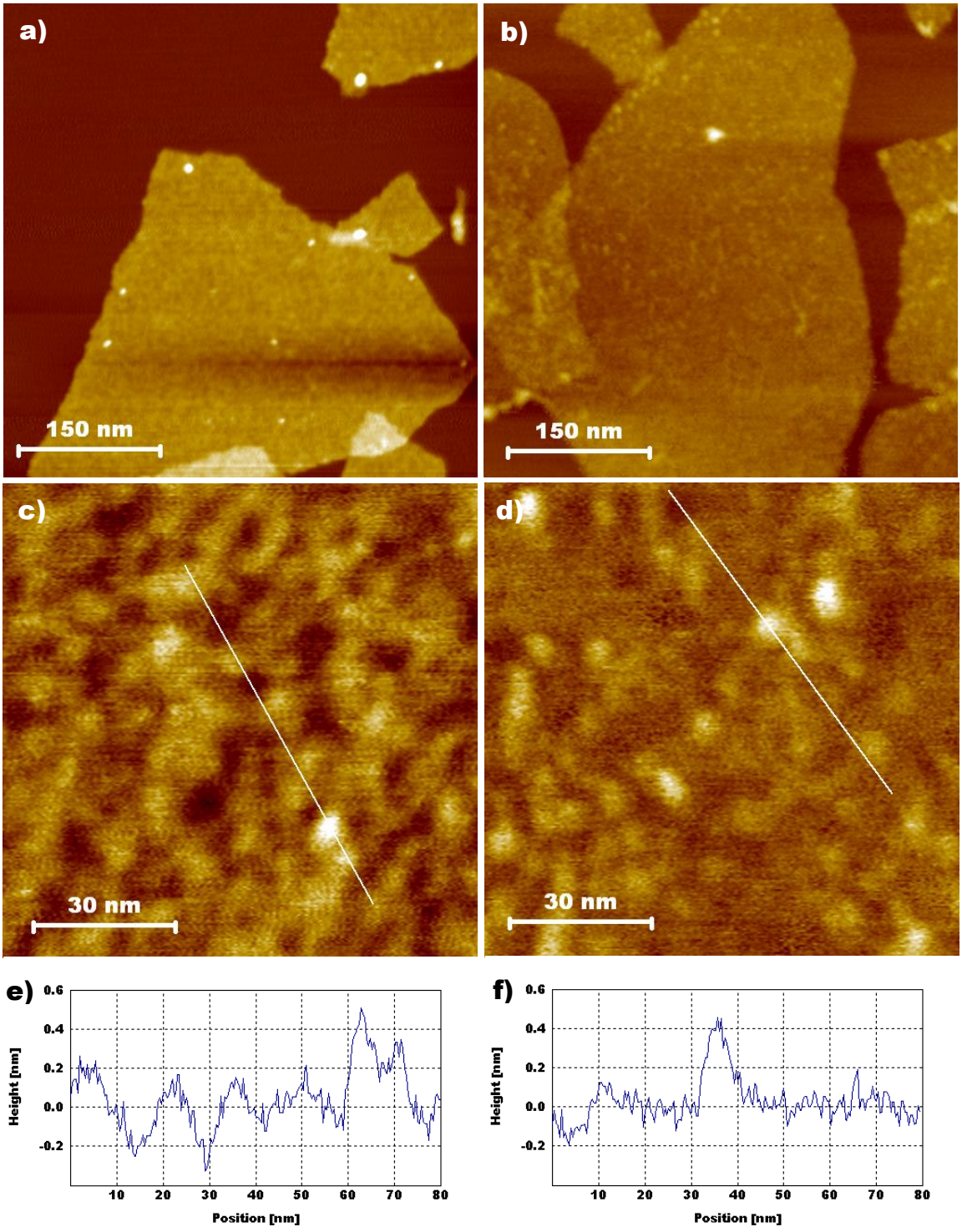

Fig. 6 Detailed tapping mode AFM height images (a-d) and line profiles (e,f) for unreduced (a,c,e) and chemically reduced (b,d,f) graphene oxide nanosheets deposited from aqueous dispersions onto freshly cleaved HOPG. The line profiles in e and f were taken from the white lines marked in c and d, respectively.

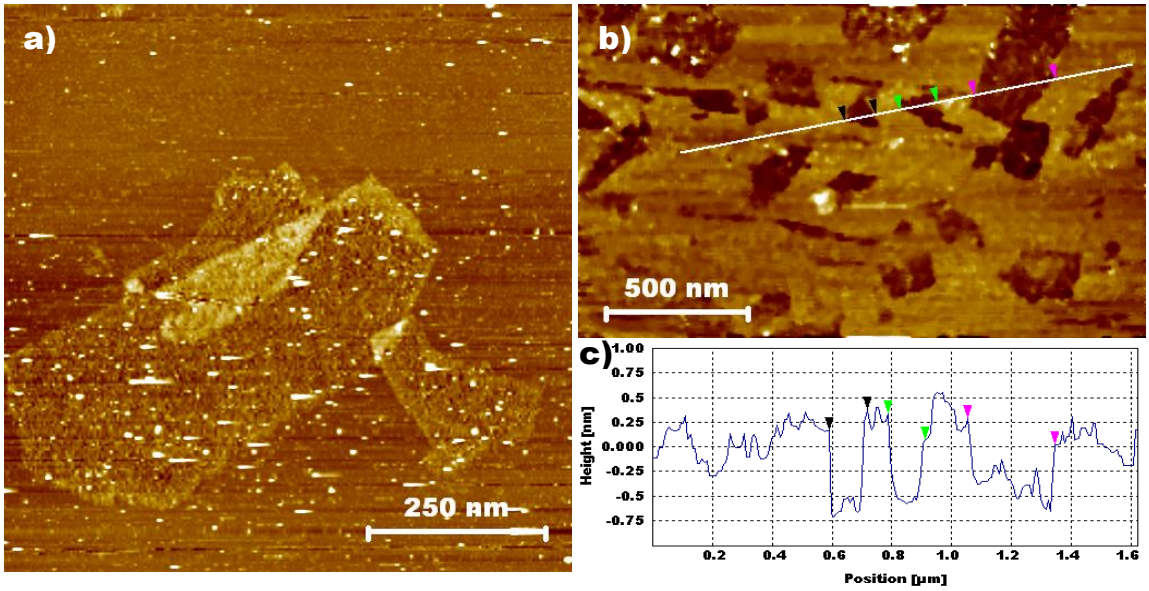

Fig. 7 STM images of unreduced graphene oxide nanosheets deposited from an aqueous dispersion onto HOPG and visualized with normal (a) and inverted (b) contrast. Tunneling parameters: I = 0.5 pA, V = -2000 mV (a); I = 1 pA, V = 2000 mV (b). (c) Line profile taken along the white line marked in (b).

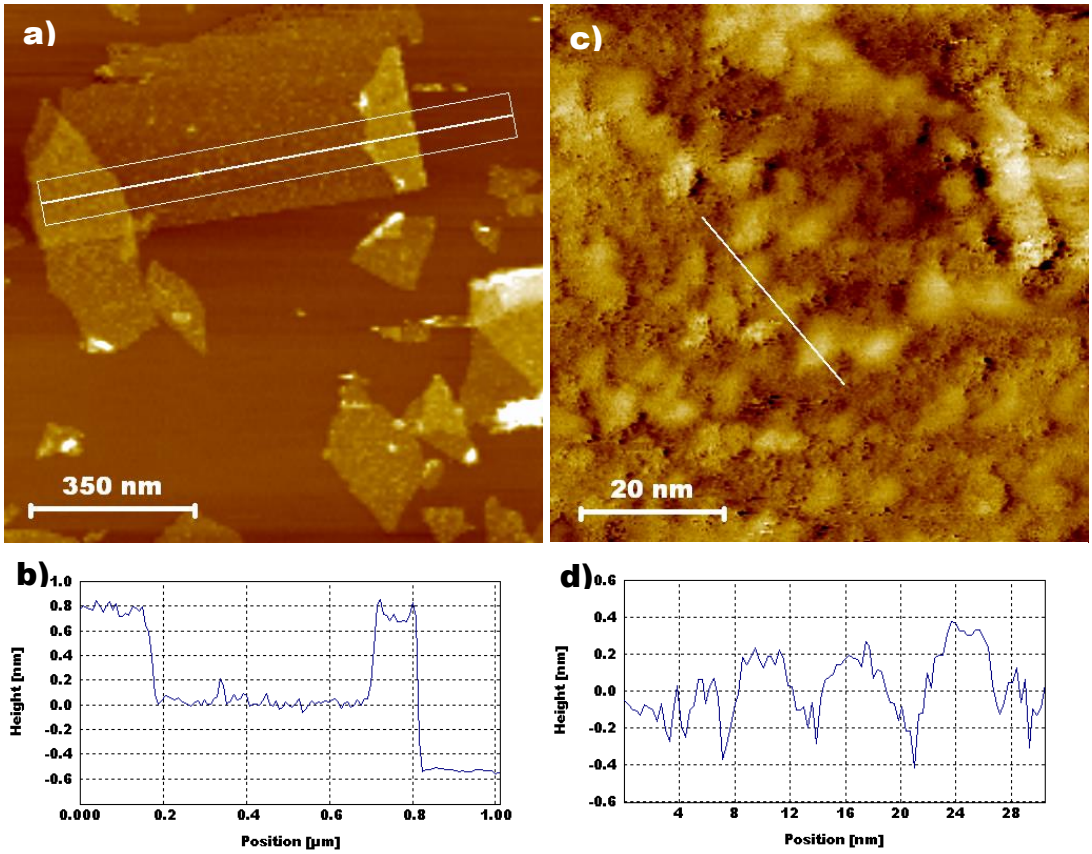

Fig. 8 Nanometer-scale STM images (a,c) and line profiles (b,d) of chemically reduced graphene oxide nanosheets deposited onto HOPG from their dispersion in water. The line profile in (b) represents the average obtained within the marked rectangle in (a), whereas that in (d) was taken along the white line marked in (c). Tunneling parameters: I = 0.5 nA, V = 100 mV (a); I = 0.5 nA, V = 500 mV (b).

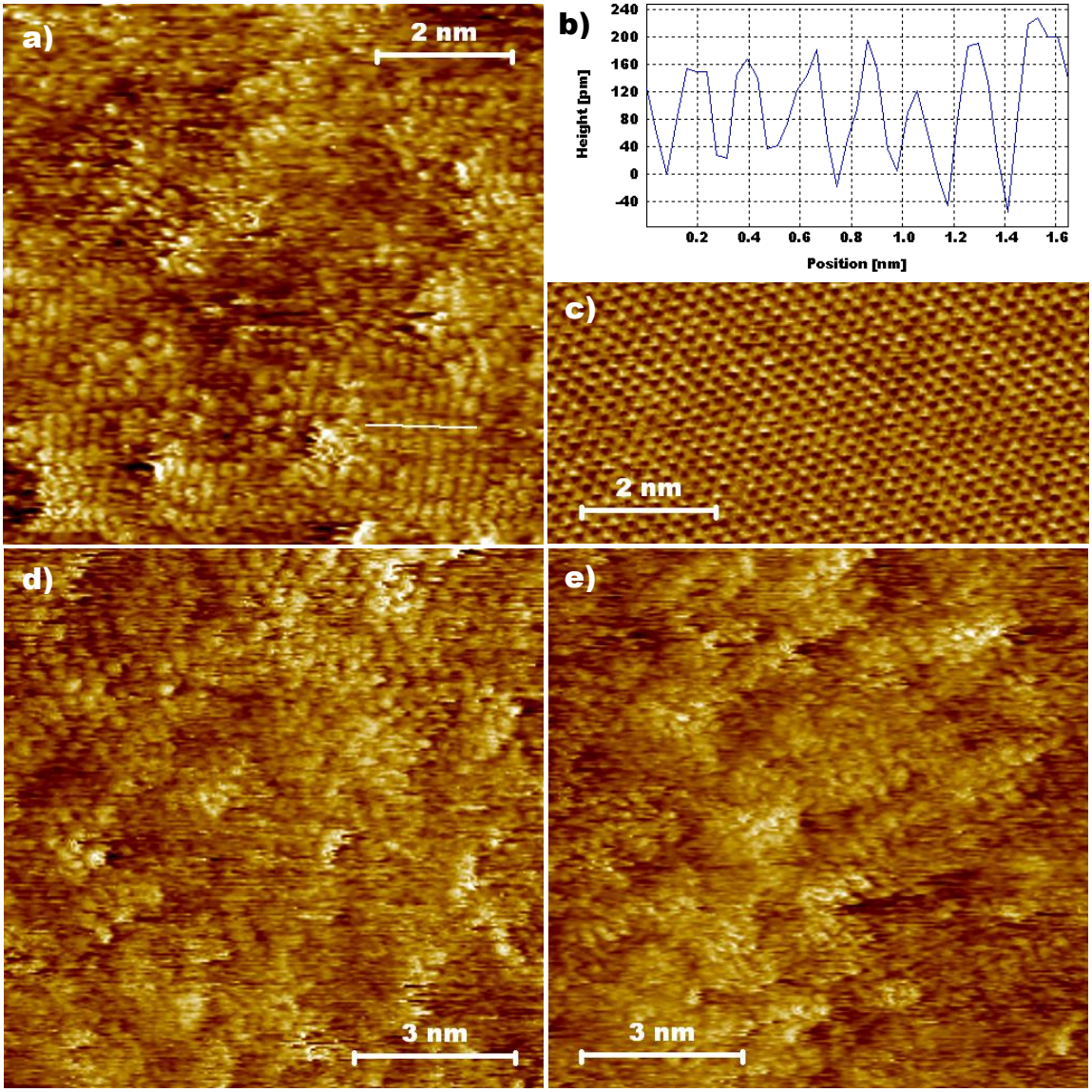

Fig. 9 Typical atomic-scale STM images (a,d,e) of the basal plane of chemically reduced graphene oxide nanosheets. (b) Line profile taken along the white line marked in a. (c) Atomic-scale STM image of pristine, defect-free HOPG shown for comparison. Tunneling parameters: I = 3 nA, V = 10 mV (a); I = 2 nA, V = 100 mV (b), I = 2 nA, V= 50 mV (c); I = 3 nA, V = 50 mV (d).

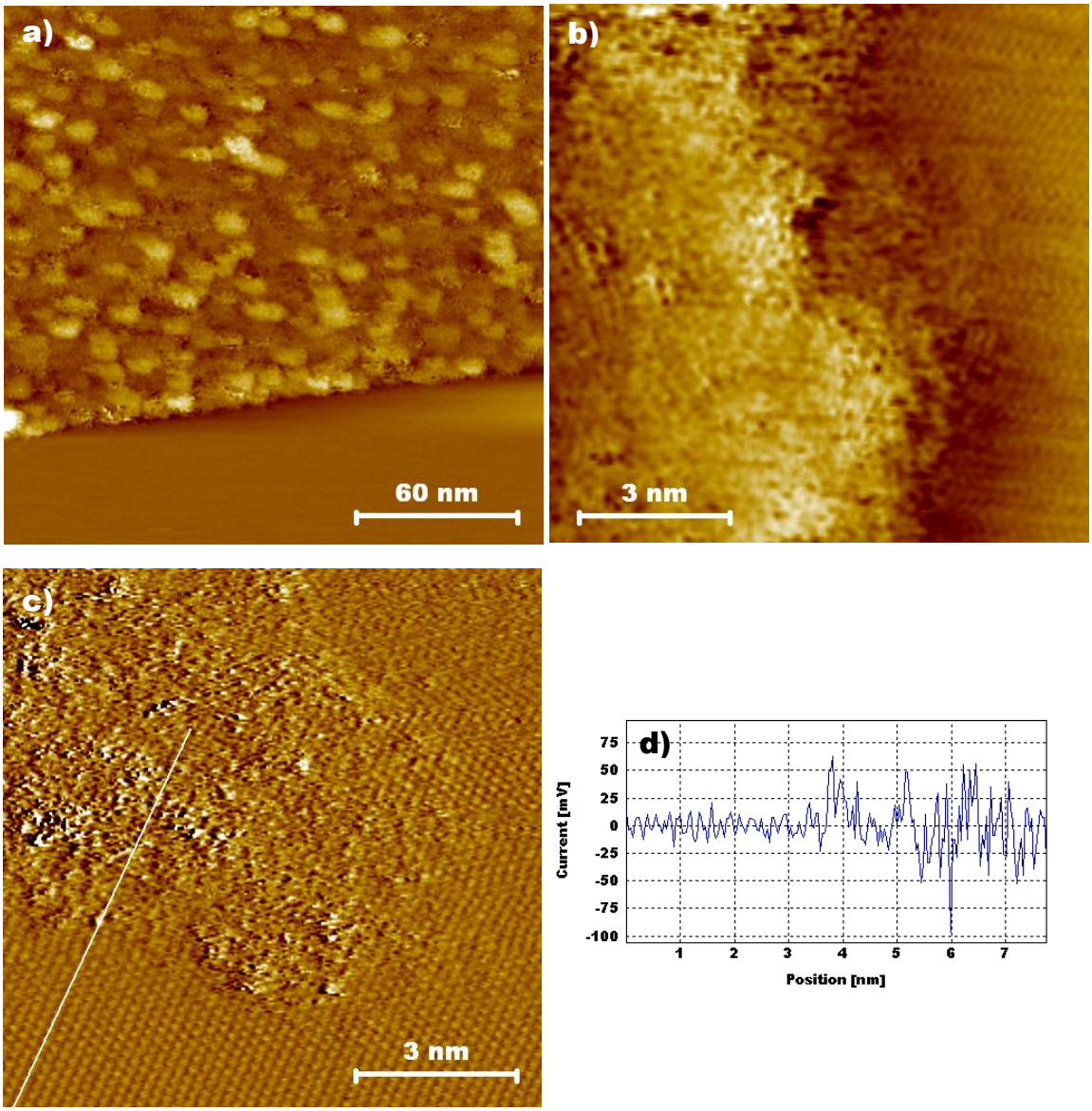

Fig. 10 STM images of the edges of chemically reduced graphene oxide nanosheets: Nanometer scale image showing the smooth, straight edge of a nanosheet (a). Atomic-scale images of a nanosheet edge (b) and a nanosheet corner (c). Image c is a current STM image. (d) Line profile taken along the white line marked in c. Tunneling conditions: I = 0.5 nA, V =100 mV (a); I = 3 nA, V = 20 mV (b); I = 3.5 nA, V = 15 mV (c).

For Table of Contents use only:

"Atomic force and scanning tunneling microscopy imaging of graphene nanosheets derived from graphite oxide"
J.I. Paredes, S. Villar-Rodil, P. Solís-Fernández, A. Martínez-Alonso, J.M.D. Tascón

Table of Contents Graphic

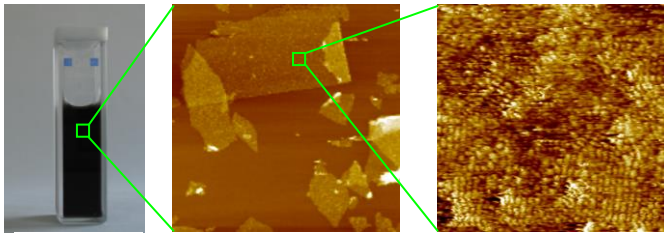

Graphene dispersion | Graphene nanosheets | Atomic-scale structure